Nonlinear dynamics and inner-ring photoluminescence pattern of indirect excitons

Mathieu Alloing,[1] Aristide Lemaître,[2] Elisabeth Galopin,[2] and François Dubin[1]
[1]*ICFO—The Institut of Photonic Sciences, Avenida Carl Friedrich Gauss, número 3, 08860 Castelldefels (Barcelona), Spain*
[2]*Laboratoire de Photonique et Nanostructures, LPN/CNRS, Route de Nozay, 91460 Marcoussis, France*
(Received 9 February 2012; revised manuscript received 23 May 2012; published 7 June 2012)

We study the photoluminescence dynamics of ultracold indirect excitons optically created in a double-quantum-well heterostructure in the regime in which the inner photoluminescence ring is formed. We show that the spectrally resolved dynamics is in agreement with an excitonic origin for the inner ring which appears due to the local heating of indirect excitons by laser excitation. To confirm this interpretation and exclude the ionization of indirect excitons, we evaluate the excitonic density that is extracted from the energy of the photoluminescence emission. It is shown that optically injected carriers play a crucial role in that context as these are trapped in our field-effect device and then vary the electrostatic potential controlling the confinement of indirect excitons. This disruptive effect blurs the estimation of the exciton concentration. However, it is suppressed by placing the double quantum well behind a superlattice where a fraction of photoinjected carriers remains trapped and then screens fluctuations of the electrostatic potential at the gate electrodes. In this improved geometry, we then estimate that the exciton density remains one order of magnitude smaller than the critical density for the ionization of indirect excitons (or Mott transition) in the regime where the inner ring is formed.

DOI: 10.1103/PhysRevB.85.245106 PACS number(s): 78.67.De, 73.63.Hs, 73.21.Fg, 78.47.jd

I. INTRODUCTION

In the quest for a model system to study ultracold dipolar gases in the solid state, semiconductor heterostructures offer a very promising route. In particular, a double quantum well (DQW) embedded in a field-effect device opens a unique opportunity to engineer and control so-called spatially indirect excitons. These dipolar quasiparticles result from the Coulomb attraction between electrons and holes that are spatially separated and confined in distinct quantum wells. This situation is achieved by applying an external electric field perpendicularly to a DQW such that the minimum-energy states for electrons and holes lie in distinct quantum wells. First, the spatial separation imposed between electronic carriers provides indirect excitons with a large electric dipole, aligned perpendicularly to the plane of the DQW, such that repulsive dipolar interactions between excitons are dominant at low temperatures. Remarkably, the dipolar repulsions yield a screening of the disorder of the semiconductor matrix[1,2] and also trigger a rapid expansion of exciton gases.[3] In addition, spatially separating electrons and holes highly reduces the overlap between the electronic wave functions. Thus, indirect excitons of double quantum wells exhibit radiative lifetimes orders of magnitude larger than those in single quantum wells. At the same time, they benefit from an efficient thermalization by the semiconductor lattice, bringing dense gases into the sub-Kelvin-temperature regime.[4,5]

In general, indirect excitons can be electrically or optically created in double quantum wells. In the latter case, microphotoluminescence experiments have revealed that indirect excitons form characteristic spatial patterns and particularly ring-shaped structures. Precisely, above a threshold laser excitation, a wide (outer) luminescence ring is observed hundreds of microns away from the excitation spot where electronic carriers are created.[6,7] In addition, a narrow (inner) luminescence ring is formed around the excitation spot itself.[6,8–10] On the one hand, it has been established that the outer ring signals the recombination between optically and electrically injected carriers.[11–14] On the other hand, the origin of the inner photoluminescence ring has first been attributed to the laser-induced heating of indirect excitons: combined experimental and theoretical studies have shown that the inner luminescence ring is the signature of the transport and subsequent cooling of the indirect excitons outside the excitation spot.[8,10,15,16] Alternatively, the appearance of the inner ring has been discussed in terms of the ionization of indirect excitons by experiments which have underlined that it is formed at the onset of the Mott transition.[9] Consequently, the exciton concentration shall be accurately estimated in the regime in which the inner ring appears. However, we show here that this can constitute a delicate task since the exciton density is deduced from the energy shift of the photoluminescence emission which depends on the field-effect device embedding the DQW and particularly on stray electric fields or charges that may be optically and/or electrically injected.

Here, we report experiments probing the dynamics of the photoluminescence emission of indirect excitons in the regime where the inner photoluminescence ring is formed. Our experiments are carried out with high spatial, spectral, and temporal resolutions at a bath temperature of 400 mK. Thus, the main characteristics of the inner ring are revealed. Within the region that is laser excited, these characteristics include nonlinear dynamics marked by a jump of the photoluminescence signal at the end of the laser pulse together with a rapid decrease of the emitted spectral linewidth. On the other hand, the photoluminescence emitted outside of the illuminated region exhibits a reduced photoluminescence jump and is also spectrally narrower, even during laser excitation. These observations are in good agreement with the works of Butov and co-workers[8,10,15,16] and suggest for our experiments that the inner ring marks the recombination of indirect excitons heated locally by the laser excitation. To confirm this interpretation, we analyzed the energy shift of the photoluminescence emission in order to quantify the exciton density in the regime where the inner ring is formed.

Thus, we show that a fraction of photoinjected carriers is trapped in our field-effect device at the Schottky barrier between our metallic gate electrode and the semiconductor heterostructure. Accordingly, the internal electric field is varied by the photoexcitation so that the photoluminescence exhibits very large energy shifts, preventing a quantitative estimation of the exciton density. In this context, we report studies of a second device where the DQW is placed behind a superlattice in which carriers can be optically injected and confined. The superlattice is used to screen fluctuations of the potential at the gate electrode. For this second device, our experiments show that the DQW heterostructure is then subject to a homogeneous electric field as the laser excitation is varied, i.e., as the concentration of photoinjected carriers is increased. In this improved situation, we estimate that the exciton density remains about an order of magnitude less than the predicted onset for the Mott transition in the regime where the inner ring arises. This allows us to conclude for our experiments that the appearance of the inner ring marks the recombination of indirect excitons.

II. EXPERIMENTAL APPARATUS AND FIELD-EFFECT DEVICE

We present in Fig. 1 the first field-effect device that we studied experimentally. It is made of a *metal-i-n* heterostructure in which a DQW constituted by two 8-nm-wide GaAs quantum wells separated by a 4-nm $Al_{0.33}Ga_{0.67}As$ barrier is placed in a $Al_{0.33}Ga_{0.67}As$ layer with a thickness equal to 1 μm. The DQW is positioned 50 nm above a Si-doped GaAs buffer ($n_{Si} \sim 10^{18}$ cm^{-3}) acting as the electrical back gate, grounded in our experiments. On the surface of the sample, a 100-μm-wide disk-shaped semitransparent electrode (Au/Ti, 4/4 nm thick) is deposited and is biased at V_g to control the electric field inside the field-effect device. Thus, our device implements a 100-μm-wide electrostatic trap for indirect excitons [see Fig. 1(d)] wherein the minimum-energy states for electrons and holes lie in separate quantum wells. In the following, a positive bias is applied to the top-gate electrode such that electrons and holes are confined in the top and bottom quantum wells, respectively [see Fig. 1(c)]. Finally, let us note that we probe a device in which the DQW is placed close to the back-gate electrode. This geometry is promising to engineer optoelectronic devices by reducing the surface electrodes' dimensions to a few micrometers while a homogeneous electric field is maintained at the position of the double quantum well.[17–20]

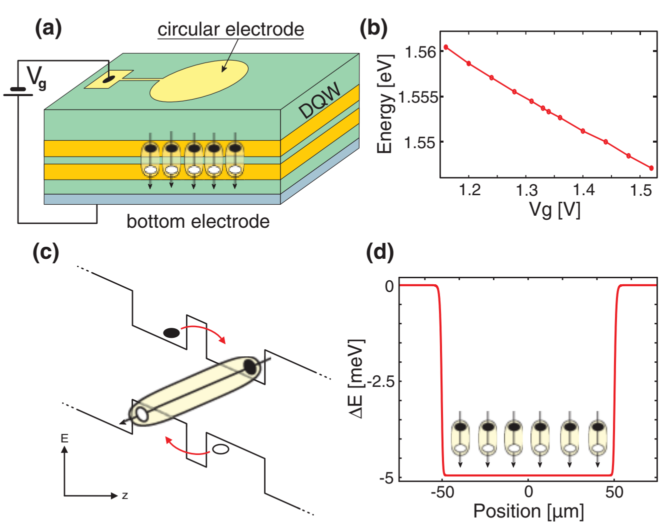

FIG. 1. (Color online) (a) Schematic representation of the field-effect device. Electrons and holes are displayed by filled and open circles, respectively. (b) Energy of the photoluminescence emission of indirect excitons as a function of the gate voltage V_g. (c) Band diagram of the DQW along the vertical direction z. (d) Trapping potential $\Delta E = d_z E_z$ created by the circular electrode for an effective applied voltage $V_g - V_s = 0.4$ V.

In the experiments presented in the following, we placed the semiconductor sample on the Helium-3 insert of a closed cycle Helium-4 cryostat (Heliox-ACV from Oxford Instruments). An aspheric lens with a 0.6 numerical aperture is embedded inside the cryostat in front of the sample and positioned by piezoelectric transducers (ML17 from MechOnics-Ag). To limit mechanical vibrations, let us note that we modified the cold head of the cryostat and introduced a mechanical coupling between the Helium-3 insert where the sample is placed and the part supporting the aspheric lens and piezoelectric transducers. Thus, mechanical vibrations have an amplitude which is decreased to about 1–2 μm (in a frequency range up to $\sim$1 KHz) while without this modification the amplitude of vibrations ranges between 5 and 10 μm. For the following experiments, indirect excitons were optically created in the electrostatic trap by a laser excitation at 640 nm. The incident-photon energy was then greater than the band gap of the GaAs layers while indirect excitons were only formed following the energy relaxation of electrons and holes in the DQW. To study the dynamics of optically created indirect excitons, we utilized a transient laser excitation with 50-ns-long laser pulses at a repetition rate of 2 MHz. The laser light was focused at the center of the electrostatic trap and had a Gaussian profile with a full width at half maximum (FWHM) of $\approx$7(1) μm. The photoluminescence emitted by the sample was collected by the aspheric lens used for photoexcitation and directed to an imaging spectrometer coupled to an intensified CCD camera (Picostar-UF from La Vision). Thus, we studied the dynamics of indirect excitons with a 2-ns time resolution, either in real space or including a spectral resolution of 200 μeV.

First, we studied the optoelectronic characteristics of our device by analyzing the photoluminescence spectrum under low laser excitation and as a function of the gate voltage V_g. We then identified the following regimes. For $V_g \leqslant V_s = 1(0.05)$ V, the energy of the direct-exciton recombination does not vary, and the photoluminescence of spatially indirect excitons is absent from the spectrum. This behavior signals that a Schottky barrier with an amplitude V_s is formed in our device at the interface between the semitransparent metallic contact and the semiconductor heterostructure. The Schottky barrier results from both the rectification of potentials at the contact and from surface states that act as impurity levels distributed in the semiconductor-forbidden gap.[21,22] Thus, for $V_g \leqslant V_s$, the potential applied to the semitransparent electrode mostly drops across the Schottky barrier, and the DQW remains effectively unpolarized. Note that our field-effect device exhibits a built-in potential that is comparable to its theoretical expectation[21] and to what has been reported with similar structures.[23] On the other hand, for $V_g \geqslant V_s$, the photoluminescence of direct excitons initially shifts to lower energies before vanishing while the emission of charged excitons appears in the spectrum. This indicates that free carriers are trapped in the DQW though we observe a photocurrent of $\leqslant$100 nA, which is a rather typical value. At the same time, the emission of indirect excitons arises and is marked by its energy that varies linearly with increasing V_g [see Fig. 1(b)]. This behavior reveals the quantum-confined Stark effect, i.e., the interaction between the electric dipole $\vec{d}$ of indirect excitons and the electric field applied in the heterostructure $\vec{E}$, which varies as $-\vec{d} \cdot \vec{E}$. For our sample design, the in-plane components of $\vec{E}$ can be neglected, leading to a confinement of the indirect excitons under the electrode with a theoretical amplitude for the trapping potential $\Delta E = d_z E_z \sim 5$ meV for an effective applied bias $V_g - V_s = 0.4$ V [see Fig. 1(d)].

III. EXPERIMENTAL RESULTS

We present in Fig. 2 the central result of our work, namely, the appearance of a ring-shaped photoluminescence above a threshold excitation of $\sim$1.8 W cm^{-2}.[24] Remarkably, this emission profile is solely observed during the laser excitation, and the ring collapses 4 ns after the laser pulse is terminated. As mentioned above, experimental studies have previously reported the formation of this pattern that is referred to as the inner ring.[6,8–10,15] To determine the mechanisms responsible for the formation of the inner ring in our experiments, we analyzed spatially and spectrally the photoluminescence. Therefore, we selected the center of the inner-ring pattern along the vertical direction (this region is marked by the semitransparent rectangle in Fig. 2 and matches the entrance slit of our imaging spectrograph) and spectrally dispersed this component to study the dynamics of the inner ring in the real-frequency space.

In Fig. 3, the spectrally resolved photoluminescence along the vertical direction at the center of the ring pattern is presented. Precisely, a sequence of images taken during and following 50-ns-long laser pulse is displayed. For each image, the vertical direction marks the spatial coordinate, and the horizontal axis marks the energy. First, we note in Fig. 3 that the inner ring is rapidly formed within the first 10 ns of the laser

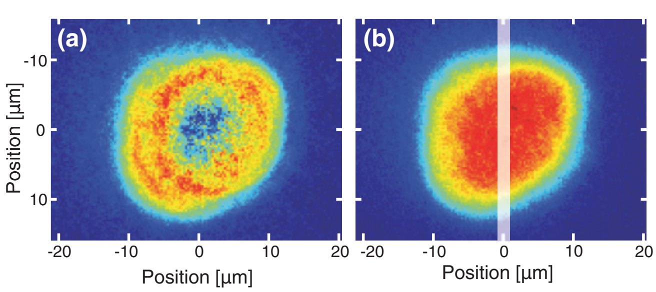

FIG. 2. (Color online) Real image of the photoluminescence emission of indirect excitons at (a) the end of the laser excitation and (b) 6 ns later. The semitransparent white region indicates the position of the entrance slit of the imaging spectrometer. The experiments were realized at a bath temperature $T_b = 400$ mK and for a laser-excitation power $P_{ex} = 14.8$ W cm^{-2}.

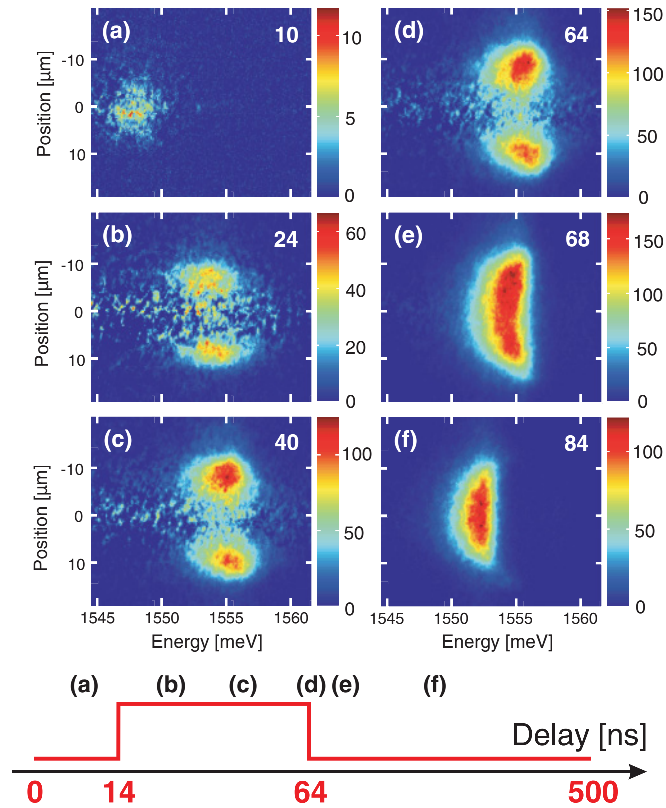

FIG. 3. (Color online) (a)–(f) Spatially resolved emission spectrum for $P_{ex} = 14.8$ W cm^{-2} recorded in 2-ns intervals at various time delays. The corresponding time delays are indicated in each image and on the schematic of the laser pulse. The intensity is color scaled independently for each spectrum. Experimental results were obtained at $T_b = 400$ mK.

pulse. Furthermore, the emission spectrally broadens during the laser excitation and reaches at the end of the laser pulse a width of $\sim$5.2 meV in the darker part (corresponding to the laser-excited region) and $\sim$4 meV for the "up" and "down" bright spots [see also Fig. 4(b)]. To examine the nature of the emission at the end of the laser excitation, let us compare the spectral widths to that emitted by an unbound-electron-hole plasma. The latter value is deduced by first estimating the density n_M at which the Mott transition occurs. It is controlled by the Bohr radius of the indirect excitons, a_B [$n_M \sim (1/a_B)$], and for our DQW we have $a_B \approx 20$ nm such that $n_M \approx 2 \times 10^{11}$ cm^{-2}. Thus, the minimum spectral width emitted by an electron-hole plasma reads $\Gamma_{e-h}^{(\min)} \sim \pi\hbar^2 n_M(1/m_e + 1/m_h)$, where m_e and m_h denote the electron and hole effective masses, respectively, and we deduce $\Gamma_{e-h}^{(\min)} \geqslant 5$ meV for our experiments. The latter value is somewhat comparable to the spectral width of the photoluminescence emitted at the center and along the perimeter of the inner ring. Thus, analyzing the photoluminescence spectral width does not provide an unambiguous determination of the nature of the emission. To establish whether the spectrally broad emission marks a significant ionization of excitons, we now discuss the dynamics of the photoluminescence once the laser excitation is switched off.

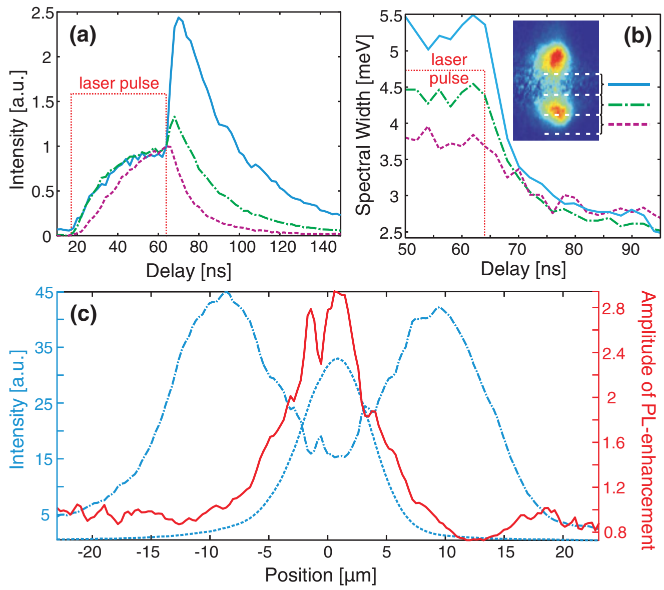

FIG. 4. (Color online) Normalized time evolution of (a) the maximum of the indirect-exciton photoluminescence and (b) the corresponding emission spectral width for $P_{\text{ex}} = 14.8$ W cm^{-2}. The blue solid, purple dashed, and green dotted-dashed lines correspond to spatial averages of the spectrum at three different positions as shown in the inset displayed in (b). Averaging is done over regions of the 7-μm width (spatial width of the excitation beam). (c) Spatial profiles of the ring-shaped photoluminescence (dotted-dashed line), excitation beam (dashed line), and PL enhancement (solid line) for $P_{\text{ex}} = 29.6$ W cm^{-2}. The PL-enhancement profile was obtained by dividing the spatial profile 4 ns after the end of the pulse (delay 68 ns) by the spatial profile at the end of the pulse (delay 64 ns).

As illustrated in Figs. 2, 3(e), and 3(f), the inner ring has distinctive dynamics and collapses in a time interval as short as a few nanoseconds after the falling edge of the laser pulse. This transition is marked by two coincident phenomena in the central region of the inner ring: a sudden enhancement of the photoluminescence signal (or PL jump) and a rapid decrease of the photoluminescence spectral width. These aspects are illustrated in Fig. 4, which displays the dynamics of the emission at the center and at two other spatial positions as depicted in the inset of Fig. 4(b). We first note in Fig. 4(a) that at the center of the inner ring, the PL jump has a far larger amplitude (up to ∼2.5) than along the bright region of the ring pattern where it reaches 1.2.[25] In fact, we note that the spatial variation of the PL jump reproduces the profile of the laser excitation as shown in Fig. 4(c). These observations well agree with the works of Butov and co-workers and then with hydrodynamical calculations predicting that the inner ring is formed due to the heating of indirect excitons induced by the laser excitation.[5,8,10,16] The PL jump marks a sharp increase of the population of the optically active lowest-energy states after the laser excitation, i.e., the rapid thermalization of the corresponding "hot" indirect excitons. On the other hand, along the circumference of the inner ring, indirect excitons are better thermalized by the semiconductor matrix, and the photoluminescence enhancement is absent or reduced. The variation of the spectral linewidth after the laser excitation further supports this interpretation [see Fig. 4(b)]. Indeed, in the central region of the inner ring, the spectral width decreases from 5.2 meV to ∼3 meV within the first 6 ns that follow the termination of the laser excitation. On the other hand, along the circumference of the inner ring, the spectral width exhibits a decrease reduced to 1 meV in the same time interval. These combined variations indicate that the inner ring is formed in a regime wherein the system is dominantly of the excitonic type. Indeed, 6 ns after the laser pulse, i.e., in a time interval during which the exciton population has weakly decreased (as shown in Fig. 7 indirect excitons exhibit an optical lifetime of ≈25 ns in the regime wherein the exciton diffusion can be neglected), the maximum spectral width lies well below $\Gamma_{e-h}^{(\text{min})}$.

Studying spatially the inner ring further supports its excitonic origin for our experiments. This is illustrated in Fig. 5 in which we present the variation of characteristic parameters as a function of the average laser intensity. These are, namely, the distance between the two local maxima of the emitted inner-ring pattern r_{ir} and the ratio between the maximum and minimum intensities V_{ir}. In Fig. 5(a), we first note that r_{ir} and V_{ir} monotonously increase with the excitation intensity; the variation of V_{ir} is consistent with an increase of the effective temperature of indirect excitons at the position of the laser excitation. Indeed, increasing the laser intensity enhances the heating induced on indirect excitons at the position of the laser excitation while outside of the illuminated region, excitons have an effective temperature that barely varies. Thus, the laser-induced heating results in a temperature gradient that controls the intensity of the emitted photoluminescence and therefore V_{ir}. In addition, the variation of r_{ir} signals that the cloud effective temperature has a spatial profile which is broadened with increasing laser intensity. It also shows that the diffusion of indirect excitons is increased with the exciton concentration as expected for repulsive dipolar interactions. In that respect, we also show in Fig. 5(b) the spatial full width at half maximum of the photoluminescence r_{c}, i.e., the extension of the exciton cloud. In the regime in which the

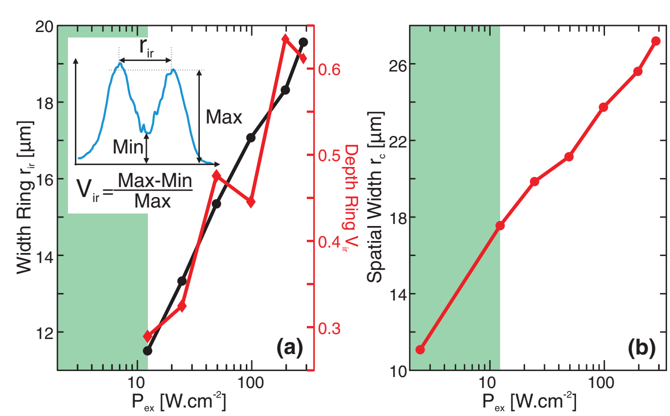

FIG. 5. (Color online) (a) Characteristics of the ring-shaped photoluminescence for various excitation powers at the end of the pulse (delay 64 ns). The black line with round markers indicates the width r_{ir} between the two maxima of the spatial profile while the red line with diamond markers indicates the depth V_{ir} of the ring as depicted in the inset. (b) Spatial width 4 ns after the end of the pulse (delay 68 ns) as a function of the excitation power. In both figures, the green shadowed region corresponds to the range of excitation power for which no ring shape can be observed.

inner ring is formed, we note that r_c increases steadily with the laser intensity. This signals that the inner ring develops in a regime wherein indirect excitons are effectively delocalized. In addition, the measurements displayed in Fig. 5(b) indicate that the expansion of the exciton cloud does not seem to vary at the onset for the formation of the inner ring. This observation contrasts with an expected steep increase of the carrier diffusion across the Mott transition[9] and then suggests that the inner ring manifests the recombination of indirect excitons for our experiments.

IV. DISCUSSION

As illustrated in Fig. 6(a), for our sample we observed that the photoluminescence signal is largely shifted towards high energies as the laser intensity is increased. We define the corresponding blue energy shift δE as the difference between the spectral position of the photoluminescence emitted at the end of the laser excitation and in the very dilute regime, i.e., following the lowest laser excitation. In Fig. 6, we note that the photoluminescence ring is observed for $4 \lesssim \delta E \lesssim 8$ meV, which we now relate to the exciton density.

Indirect excitons of the DQW constitute well oriented electric dipoles so that repulsive dipole-dipole interactions between excitons induce a shift of the photoluminescence towards higher energies. The resulting energy shift is *a priori*, directly related to the exciton density;[26] indeed, the mean-field energy associated to repulsive exciton-exciton interactions scales as $u_0 n_{2D}$, where n_{2D} is the exciton concentration in two dimensions and u_0 is a constant factor controlled by the DQW geometry and the correlations between excitons.[27,28] In Fig. 6(b), we present the exciton concentration that can be deduced from the blue energy shift, taking into account the screening of exciton-exciton interactions (see Ref. 29 for more details). This approach predicts that the highest exciton density reaches $\approx 10^{11}$ cm^{-2} for our experiments, which is somewhat close to the density range at which the Mott transition is expected ($\approx 2 \times 10^{11}$ cm^{-2}). However, we show in the following that in our experiments δE does not reflect directly the density of indirect excitons but rather the role of optically injected carriers that are trapped in the field-effect device.

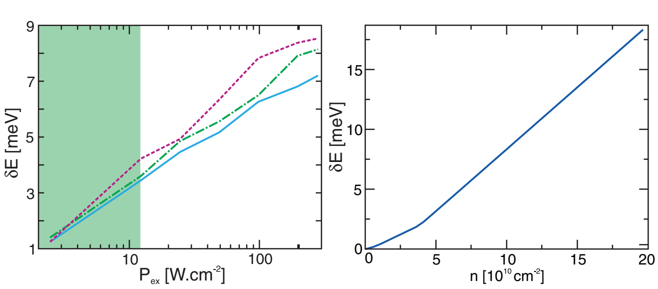

FIG. 6. (Color online) (a) Blue energy shift of the indirect-exciton photoluminescence as a function of the excitation power and measured 4 ns after the end of the laser pulse (delay 68 ns). The three lines correspond to the three spatial averages shown in Fig. 4. The reference for the shift is the energy position of the indirect-exciton line at the lowest excitation power and 100 ns after the end of the pulse. (b) Theoretical exciton density as a function of the blue energy shift for a bath temperature of 400 mK.

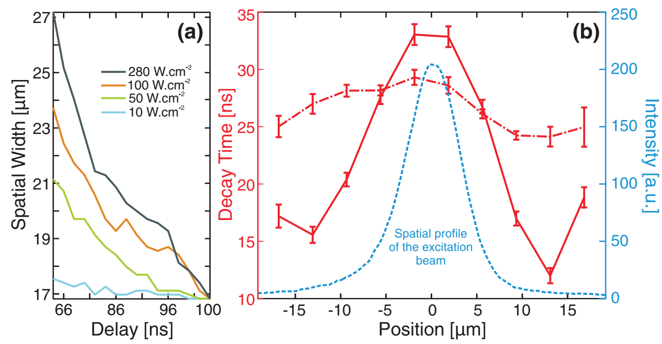

FIG. 7. (Color online) (a) Time evolution of the spatial width of the photoluminescence emission as a function of the excitation power. (The lines organize themselves from bottom to top with increasing excitation power). (b) Spatially resolved decay time for $P_{ex} = 1.8$ W cm^{-2} (red dotted-dashed line) and $P_{ex} = 29.6$ W cm^{-2} (red solid line), which are below and above the excitation threshold for the appearance of the inner ring, respectively. Decay times are calculated with a single exponential fit for a slice with a width of 3.75 μm (approximately half of the laser spatial width). The spatial profile of the excitation beam is displayed in the blue dashed line for the sake of comparison.

As mentioned previously, our experiments rely on a laser excitation at an energy greater than the band gap of the GaAs layers. This results in the injection of free carriers, most of which generate a photocurrent ($\approx$50 nA). A small fraction of optically injected carriers may also remain trapped in the device, particularly at the Schottky contact wherein a potential barrier and gap states are formed.[21,22] The capture of photoinjected carriers is underlined by the spatial dependence of the photoluminescence energy: while we expect that the photoluminescence is emitted at a higher energy at the position of the laser spot, thus reflecting a higher concentration of indirect excitons, we observe the opposite behavior in Fig. 3 with photoluminescence emitted at an energy which increases with the distance to the center of the laser excitation. This variation for the photoluminescence energy is observed during the laser excitation but also long after [see Fig. 3(e)]. The dynamics of the exciton cloud after the laser excitation suggests that this behavior is consistent with a trapping of optically injected carriers that increases the amplitude of the electric field in the laser-excited region. Indeed, while in the low-excitation regime the photoluminescence exhibits a decay time which barely varies across the exciton cloud, we note in Fig. 7(b) that the optical lifetime varies strongly in the regime wherein the inner ring is formed, compared to the low-excitation regime. Precisely, the optical-decay time increases from $\approx$27 to 32 ns in the laser-excited region while outside of the laser spot it decreases from $\approx$25 to 15 ns. We attribute this behavior to the diffusion of indirect excitons towards the region that is illuminated. This interpretation is well supported by the variation of the spatial extension of the exciton cloud as a function of the laser-excitation power. Indeed, Fig. 7(a) shows that the spatial extension of the emission rapidly shrinks after the laser pulse with a characteristic time which decreases as the excitation power increases. These combined observations signal the collection of indirect excitons towards the region that is laser excited and in which the electric field is increased. Indirect excitons being high-field seekers, the optical excitation results in the creation of an additional trapping potential. From the spatial-emission profile displayed in Figs. 3(e) and 3(f), we estimate that the optically induced trap has a depth of ∼1 meV, adding to the box-like trap (with a theoretical 5-meV depth) created by the semitransparent gate electrode.

To confirm experimentally that the large values of δE reported previously are due to the trapping of optically injected carriers, we probed a second field-effect device in which a superlattice is placed between the DQW and the top-gate electrode. The superlattice consists of 30 pairs of GaAs/AlAs layers with thicknesses equal to 3 and 1 nm, respectively, and positioned 410 nm under the semitransparent metallic contact. The architecture of the device is otherwise identical to the one shown in Fig. 1. The superlattice is incorporated to confine a fraction of optically injected carriers. Thus, a bidimensional plane of charges is formed and can screen the fluctuations of the potential at the top-gate electrode which are induced by the laser excitation.

For the second field-effect device, we first confirmed that the inner ring is formed above an excitation threshold of ∼4.9 W cm^{-2}, which is of the same order of magnitude as that of the first sample. However, it exhibits distinct spectroscopic signatures, which are summed up in Fig. 8. First, we show in Fig. 8(d) the energy shift of the photoluminescence as a function of the laser intensity under the same experimental conditions as those of the experiments shown in Fig. 4(b). In general, we note that δE is strongly reduced by the inclusion of the superlattice; it reaches at most 2.8 meV for the highest laser excitation. This value corresponds to an exciton density of $\sim 5 \times 10^{10}$ cm^{-2}, i.e., well below the threshold for the Mott transition. Also, during the laser excitation, i.e., when the inner ring is present, we observe that δE decreases with the distance to the laser excitation. This behavior contrasts with the response of our first sample and is consistent with an exciton concentration that decreases with the distance to the laser excitation [see Fig. 8(a)]. Moreover, the spectral width emitted at the center of the inner ring varies from ∼4.2 to ∼2.2 meV between the end of the laser pulse and 10 ns later. On the other hand, it remains narrower along the circumference of the inner ring and reaches 3.7 meV at the end of the laser pulse and 2.2 meV 10 ns later. Finally, after the laser pulse, we note that the photoluminescence is emitted at the same energy all across the exciton cloud [see Figs. 8(b) and 8(c)]. This signals that the electric field applied onto the DQW is spatially homogeneous. Indeed, we do not observe any spatial variation of the photoluminescence lifetime unlike for the first device. For the latter, we thus conclude that the internal electric field was varied by optically injected carriers accumulated at the Schottky contact.

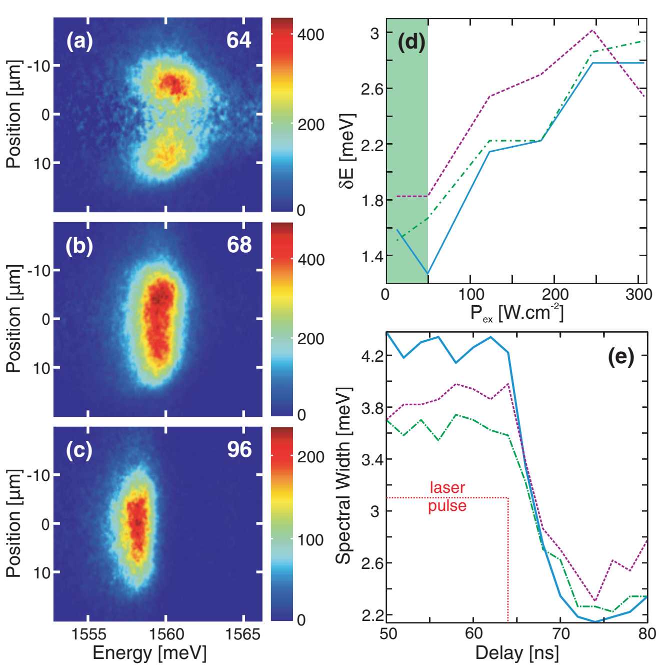

FIG. 8. (Color online) (a)–(c) Spatially resolved emission spectrum for $P_{ex} = 18.4$ W cm^{-2} recorded in 2-ns intervals at various time delays for the second field-effect device. The corresponding time delays are indicated on each image. The intensity is color scaled independently for each spectrum. (d) Blue energy shift 4 ns after the end of the pulse (68 ns) as a function of the excitation power and for the same three spatial averages as the ones shown in Fig. 4. (e) Time evolution of the spectral width for $P_{ex} = 12.3$ W cm^{-2} for the same slices mentioned above. Experiments were realized at a bath temperature $T_b = 400$ mK.

V. SUMMARY AND CONCLUSIONS

In summary, we have studied the dynamics of optically created indirect excitons in the regime wherein the inner photoluminescence ring is formed. Our experiments confirm that at the position of the laser excitation, the inner ring is marked by a sudden increase of the photoluminescence intensity at the end of the laser pulse coincident with a large decrease of the luminescence spectral linewidth. On the other hand, outside of the laser spot the photoluminescence intensity varies weakly after the laser excitation. These observations indicate that the inner ring is induced by a heating of indirect excitons locally applied by the laser excitation. To further confirm this interpretation, we have studied the exciton density created in our experiments. We have then underlined the role of optically injected carriers which remain trapped at the Schottky contact of the field-effect device where the DQW is embedded. These then vary the internal electric field, and accordingly, the relation between the blue energy shift of the photoluminescence and the exciton density is blurred. We have then shown that incorporating a superlattice between the DQW and the gate electrode efficiently reduces the influence of photoinjected carriers and allows us to estimate that the exciton concentration is about an order of magnitude lower than the threshold for the Mott transition in the regime wherein the inner ring is formed. To conclude, we would like to emphasize that despite its disruptive effect, the trapping of optically injected carriers may provide a new route to realize optically controlled microscopic traps for indirect excitons.

ACKNOWLEDGMENTS

M.A. and F.D. are grateful to M. Lewenstein and J. Eschner. This work was supported financially by the Spanish MEC (QOIT, TOQATA) and by the ERC AdG QUAGATUA while F.D. acknowledges support from the Ramon y Cajal program.

[1] M. Remeika, J. C. Graves, A. T. Hammack, A. D. Meyertholen, M. M. Fogler, L. V. Butov, M. Hanson, and A. C. Gossard, Phys. Rev. Lett. **102**, 186803 (2009).
[2] M. Alloing, A. Lemaître, and F. Dubin, Europhys. Lett. **93**, 17007 (2011).
[3] X. P. Vögele, D. Schuh, W. Wegscheider, J. P. Kotthaus, and A. W. Holleitner, Phys. Rev. Lett. **103**, 126402 (2009).
[4] A. L. Ivanov, P. B. Littlewood, and H. Haug, Phys. Rev. B **59**, 5032 (1999).
[5] A. L. Ivanov, J. Phys.: Condens. Matter **16**, S3629 (2004).
[6] L. V. Butov, A. C. Gossard, and D. S. Chemla, Nature (London) **418**, 751 (2002).
[7] D. Snoke, S. Denev, Y. Liu, L. Pfeiffer, and K. West, Nature (London) **418**, 754 (2002).
[8] A. L. Ivanov, L. E. Smallwood, A. T. Hammack, S. Yang, L. V. Butov, and A. C. Gossard, Europhys. Lett. **73**, 920 (2006).
[9] M. Stern, V. Garmider, E. Segre, M. Rappaport, V. Umansky, Y. Levinson, and I. Bar-Joseph, Phys. Rev. Lett. **101**, 257402 (2008).
[10] A. T. Hammack, L. V. Butov, J. Wilkes, L. Mouchliadis, E. A. Muljarov, A. L. Ivanov, and A. C. Gossard, Phys. Rev. B **80**, 155331 (2009).
[11] L. V. Butov, L. S. Levitov, A. V. Mintsev, B. D. Simons, A. C. Gossard, and D. S. Chemla, Phys. Rev. Lett. **92**, 117404 (2004).
[12] S. Yang, L. V. Butov, L. S. Levitov, B. D. Simons, and A. C. Gossard, Phys. Rev. B **81**, 115320 (2010).
[13] R. Rapaport, G. Chen, D. Snoke, S. H. Simon, L. Pfeiffer, K. West, Y. Liu, and S. Denev, Phys. Rev. Lett. **92**, 117405 (2004).
[14] B. Fluegel, K. Alberi, L. Bhusal, A. Mascarenhas, D. W. Snoke, G. Karunasiri, L. N. Pfeiffer, and K. West, Phys. Rev. B **83**, 195320 (2011).
[15] Y. Y. Kuznetsova, J. R. Leonard, L. V. Butov, J. Wilkes, E. A. Muljarov, K. L. Campman, and A. C. Gossard, arXiv:1202.3096.
[16] A. L. Ivanov, Europhys. Lett. **59**, 586 (2002).
[17] A. T. Hammack, N. A. Gippius, S. Yang, G. O. Andreev, L. V. Butov, M. Hanson, and A. C. Gossard, J. Appl. Phys. **99**, 066104 (2006).
[18] R. Rapaport, G. Chen, S. Simon, O. Mitrofanov, L. Pfeiffer, and P. M. Platzman, Phys. Rev. B **72**, 075428 (2005).
[19] G. Chen, R. Rapaport, L. N. Pfeiffer, K. West, P. M. Platzman, S. Simon, Z. Vörös, and D. Snoke, Phys. Rev. B **74**, 045309 (2006).
[20] A. A. High, A. K. Thomas, G. Grosso, M. Remeika, A. T. Hammack, A. D. Meyertholen, M. M. Fogler, L. V. Butov, M. Hanson, and A. C. Gossard, Phys. Rev. Lett. **103**, 087403 (2009).
[21] J. Tersoff, Phys. Rev. Lett. **52**, 465 (1984).
[22] H. Luth, *Solid Surfaces, Interfaces, and Films* (Springer-Verlag, Berlin, 2001).
[23] G. J. Schinner, E. Schubert, M. P. Stallhofer, J. P. Kotthaus, D. Schuh, A. K. Rai, D. Reuter, A. D. Wieck, and A. O. Govorov, Phys. Rev. B **83**, 165308 (2011).
[24] The calibration of the excitation power is done considering that 99% of the power is contained in a disk of radius $\sim$1.23 times the laser spatial FWHM, the laser beam having a Gaussian profile.
[25] We define the amplitude of the PL jump as the ratio between the maximum of the spectrum detected 4 ns after the end of the laser pulse, i.e., at delay 68 ns, and at the end of it, i.e., at delay 64 ns.
[26] S. B. de Leon and B. Laikhtman, Phys. Rev. B **63**, 125306 (2001).
[27] C. Schindler and R. Zimmermann, Phys. Rev. B **78**, 045313 (2008).
[28] B. Laikhtman and R. Rapaport, Phys. Rev. B **80**, 195313 (2009).
[29] A. L. Ivanov, E. A. Muljarov, L. Mouchliadis, and R. Zimmermann, Phys. Rev. Lett. **104**, 179701 (2010).